Acta Mech 233, 4063–4081 (2022)
https://doi.org/10.1007/s00707-022-03313-4

ORIGINAL PAPER

Kostas D. Housiadas · **Christos Tsangaris**

High-order lubrication theory in channels and tubes with variable geometry

Received: 21 January 2022 / Revised: 21 June 2022 / Accepted: 18 July 2022 / Published online: 1 September 2022

Abstract Lubrication theory is used widely due to its simplicity and accuracy in many circumstances such as for the modeling of thin fluid films, the motion of particles near surfaces, and the flow in narrow geometries and configurations. Here, we present an extension to the classical lubrication theory to study the laminar flow of an incompressible and highly viscous simple Newtonian fluid in microfluidic channels and tubes with variable geometry using a formal perturbation expansion in terms of the aspect ratio. The analysis generalizes and extends the work of Tavakol et al., Proc. R. Soc. A, 473 (2017) by considering (a) different shapes for the upper and lower walls of the channel, and (b) axisymmetric tubes with variable circular cross section. Analytical expressions in series form for the average pressure drop, required to maintain the constant flowrate through the channel or tube, are derived, where the formulas are provided in terms of the function(s) that describe the shape of the wall(s). Furthermore, the formulas are processed with techniques that increase the accuracy and extend the domain of convergence of series. For symmetric and periodic undulating channels and tubes, the comparison of the analytical results derived here with numerical results from the literature reveals the great accuracy and efficiency of the high-order lubrication theory, as well as its superiority against the well-known domain perturbation method.

1 Introduction

In the theory of Newtonian fluid mechanics various techniques have been developed through the years in order to find approximate analytical solutions of the relevant governing equations. For laminar highly viscous flows in narrow geometries and confined configurations with slow changes in curvature, a well-known technique is the classical lubrication approximation (or lubrication theory) [1–3]. The lubrication theory allows for the derivation of analytical approximate solutions of the Navier–Stokes equations at low Reynolds numbers. Due to its simplicity and its acceptable accuracy, even beyond the formal limits of validity, it has been used widely to describe the field variables (velocity and pressure) of film lubricants [4, 5], the motion of particles within a fluid and near boundaries [6, 7], the fluid flow in microchannels with known geometry [8–11], the flow driven by contracting walls of microchannels and microtubes [12–14], and the flow of thin liquid films with free surfaces [15–19]. The lubrication theory is valid in all these cases provided that the magnitude of the boundary slope is sufficiently small so that the induced variations of the field variables along the main flow direction are much smaller than the variations along the direction normal to the solid boundary.

In the case of narrow and confined geometries, one of the main interests is to understand the relationship between the imposed flow-rate and pressure drop for a given geometry, while another important factor which also affects this relationship is the rheology of the fluid (not considered here though); see for instance Boyko and Stone [20] and references therein. Indeed, the pressure drop is of great significance in a large variety of

K. D. Housiadas (✉) · C. Tsangaris
Department of Mathematics, University of the Aegean, 83200 Karlovassi, Samos, Greece
e-mail: housiada@aegean.gr

physical processes and applications such as the design and manufacturing of microfluidic devices with soft or deformable materials [21–26], the modelling of multiphase fluid–structure interactions in industrial piping and turbomachinery [27], the understanding of the mechanics of blood flow in microvessels, arteries and veins [28–31], and in medical applications such as the precise estimation of the injection force of subcutaneous drug administration [32, 33], to name only a few.

Tavakol et al. [34] studied the flow of a simple Newtonian fluid in a channel with a variable but fixed *a-priori* boundary. The goal was to study the effect of a large constriction made by a trapped cell, particle, bubble or droplet, or as a result of buckled, crumpled or swollen walls. The shape of the upper wall of the channel was described mathematically by any continuous and differentiable, or piecewise differentiable, function $H = H(x)$ where x is the distance from the inlet plane. Provided that the curvature of the boundary is modest, Tavakol et al. [34] calculated analytically the first and second correction terms to the leading-order approximation. Strictly speaking, the leading-order approximation is valid in the limit of a vanishing small aspect ratio $\delta \equiv h_0/L_0$ (i.e., for $\delta << 1$, or $\delta \to 0^+$) where h_0 is the channel height and $2L_0$ is the length of the channel. The higher-order terms extend the classical leading-order lubrication solution, and relax the main limitation of the theory, which is the vanishing small aspect ratio. Comparison of the analytical, high-order results with experimental results as well as with direct numerical solutions of the Navier–Stokes equations showed that the higher-order terms improve substantially the accuracy of the leading-order solution. In a more recent work, Hinojosa et al. [35] investigated a general serpentine channel with different shapes for the upper and lower walls in Cartesian geometry and found the solution of the Stokes equations up to second-order in the aspect ratio of the channel.

In this paper, we follow the work of Tavakol et al. [34] and extend their systematic and successful analysis which involves corrections to the leading-order lubrication solution [10, 36–38] in order to study a channel with two variable walls in Cartesian geometry, as well as an axisymmetric tube with variable cross section in cylindrical geometry. In both cases, the shape of the wall(s) is fixed and described with smooth, continuous and adequately differentiable functions. Our method of solution is a formal regular perturbation technique in terms of the aspect ratio of the channel or tube. This method appears to be superior to the domain perturbation method [2, 39–45], which can be used when the amplitude of the variation of the boundary is much smaller than the channel height. One is reminded that according to the domain perturbation method, the expansion parameter for the solution of the governing equations is the ratio of the amplitude of the curvature of the boundary to the channel height (or radius of the tube), while in the classical lubrication theory, and in the extended lubrication theory used here, the expansion parameter is the ratio of the channel height (or radius of the tube) to the total length of the duct (channel or tube). On the contrary, the high-order lubrication theory is suitable even for constrictions whose amplitude approaches the channel height [34]. We also note that in the Cartesian geometry our formulation gives the possibility to investigate fully asymmetric channels with different boundary shapes or different constrictions imposed on the walls of the channel.

The rest of the paper is organized as follows. In Sect. 2, we give the governing equations and the accompanying auxiliary (boundary and integral) conditions for the steady laminar flow of an incompressible and highly viscous Newtonian fluid in a channel with two variable walls. The method of solution, the procedure for the derivation of the solution, and the analytical solution are provided in this Section, too. In Sect. 3, we study the axisymmetric flow in a tube with variable cross section following the same structure as in Sect. 2. In Sect. 4, we present the most interesting results focusing on the average pressure drop which is required to maintain the constant flowrate through the channel or tube. The pressure drop is derived and presented in terms of the shape function(s); we also employ and discuss specific examples for the shape functions. Finally, in Sect. 5 we state our conclusions.

2 Flow in a channel

We consider the isothermal and incompressible steady flow of a simple Newtonian fluid in a two-dimensional channel, the walls of which can vary smoothly as function of the distance from the inlet plane. The length of the channel is l, and the distance between the walls at the inlet is h_0. We use a Cartesian coordinate system $x^* y^* z^*$ to describe the flow field, where x^* is the main flow direction, y^* is direction between the two walls and vertical to the x^*-direction, and z^* is the neutral direction, normal to the x^* y^*-plane (throughout the text, a superscript * denotes a dimensional quantity). The origin of the coordinate system is located in the middle of the inlet plane such that the distance to each wall is $h_0/2$; see Fig. 1a. The walls of the channel are allowed to have different shapes; the upper wall is described by the shape function $H^* = H^*(x^*)$ and the lower wall by $\Phi^* = \Phi^*(x^*)$. Based on the shape functions the upper wall is given as $F_u^*(x^*, y^*) = y^* - H^*(x^*) = 0$,

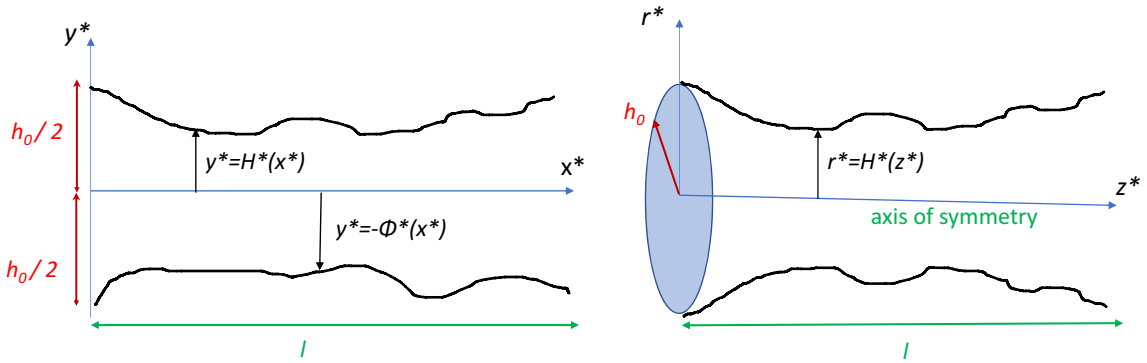

Fig. 1 (**a**) Geometry and Cartesian coordinate system x^*y^* for a general channel with two varying walls, (**b**) geometry and cylindrical coordinate system r^*z^* for an axisymmetric tube with a circular cross-section varying with the distance z^* from the inlet

while the lower wall is given as $F_l^*(x^*,\ y^*) = y^* + \Phi^*(x^*) = 0$. The choice of the coordinate system and the fact that the flow is possible as long as the two walls are not joined imply that the shape function must meet the requirements: $H^*(x^* = 0) = \Phi^*(x^* = 0) = h_0/2 > 0$ and $H^*(x^*) + \Phi^*(x^*) > 0$ for any $x^* \in [0,\ \ell]$. The velocity vector in the flow domain is denoted by $\mathbf{u}^* = u_x^*\mathbf{e}_x + u_y^*\mathbf{e}_y$ ($\mathbf{e}_x$, $\mathbf{e}_y$ are the units vectors in the x^*, y^*, directions, respectively), and the total pressure is denoted by p^*; the latter is induced by the imposed flow-rate q (per unit length in the neutral direction) at the inlet plane, i.e., $q = \int_{-h_0/2}^{h_0/2} u_x^*(0,\ y^*)dy^*$.

In the absence of inertia and any external forces and torques, the fluid motion in the channel is governed by the mass balance (continuity equation), the momentum balance, and the Laplacian equation for the pressure:

$$\nabla \cdot \mathbf{u}^* = 0, \quad -\nabla p^* + \mu\,\nabla^2\mathbf{u}^* = \mathbf{0}, \quad \nabla^2 p^* = 0 \tag{1.1–3}$$

where μ is the constant shear viscosity of the fluid. Note that Eq. (1.3) is not an independent equation. It has been derived by taking the divergence of Eq. (1.2) and using the continuity equation, Eq. (1.1). The domain of definition of Eqs. (1) is $\Omega_{cart} = \{(x^*,\ y^*)|0 < x^* < \ell,\ -\Phi^*(x^*) < y^* < H^*(x^*)\}$. Equations (1.1–3) are accompanied with the usual no-slip and no-penetration boundary conditions along the channel walls, $\mathbf{u}^* = \mathbf{0}$ at $y^* = H^*(x^*)$ and $y^* = -\Phi^*(x^*)$, along with the integral constraint, i.e., the total mass balance, $q = \int_{-\Phi^*(x^*)}^{H^*(x^*)} u_x^*(x^*,\ y^*)dy^*$.

We introduce dimensionless variables based on the lubrication theory, i.e., $X = X^*/X_c$ where $X = x$, y, u_x, u_y, p, H, Φ, and X_c is the relevant characteristic scale for X^*. First, the characteristic scale in the x^*-direction is ℓ, and the characteristic scale in the y^*-direction is h_0. The shape functions H^* and Φ^* are scaled with h_0, too. Using the mass flow-rate at the inlet plane ($x^* = 0$) one finds that the characteristic scale for the velocity component in the main flow direction is q/h_0. Then, with the aid of the continuity equation one finds that the characteristic scale for the velocity component in the y^*-direction is q/ℓ. Last, from the component of the momentum balance in the main flow direction, we find that the suitable characteristic scale for the pressure is $\mu\, q\, \ell/h_0^3$. Thus, the final dimensionless governing equations in scalar form are:

$$\frac{\partial u_x}{\partial x} + \frac{\partial u_y}{\partial y} = 0, \tag{2}$$

$$-\frac{\partial p}{\partial x} + \varepsilon^2\frac{\partial^2 u_x}{\partial x^2} + \frac{\partial^2 u_x}{\partial y^2} = 0, \tag{3}$$

$$-\frac{\partial p}{\partial y} + \varepsilon^4\frac{\partial^2 u_y}{\partial x^2} + \varepsilon^2\frac{\partial^2 u_y}{\partial y^2} = 0, \tag{4}$$

$$\frac{\partial^2 p}{\partial y^2} + \varepsilon^2\frac{\partial^2 p}{\partial x^2} = 0 \tag{5}$$

where $\varepsilon \equiv h_0/\ell$ is the aspect ratio of the channel (recall that $h_0 = H^*(0) + \Phi^*(0)$). The auxiliary (boundary and integral) conditions are:

$$u_x = u_y = 0 \quad \text{at } y = -\Phi(x) \text{ and } H(x),\ \ 0 \le x \le 1, \tag{6}$$

$$\int_{-\Phi(x)}^{H(x)} u_x(x,y)dy = 1. \tag{7}$$

Equation (7) simply results from the integration of Eq. (2) along the y-direction between the limits $y = -\Phi(x)$ and $y = H(x)$, applying the no-penetration condition at the channel walls, and using the dimensionless flow-rate at the inlet plane, i.e., $\int_{-1/2}^{1/2} u_x(0,\ y)dy = 1$ where, due to the characteristic scales used above, $H(0) = \Phi(0) = 1/2$. Note that the shape functions H and Φ are considered known in advance. For $H(x) = \Phi(x) = 1/2$ one gets a straight channel, while for $\Phi(x) = 1/2$ the physical problem reduces to that studied in Ref. [34] (see also below in Sect. 4).

2.1 Method of solution and solution procedure

Equations (2, 3,4, 5, 6, and 7) only involve one dimensionless parameter, the aspect ratio of the channel ε, which appears in the equations in even powers. When the square of the aspect ratio is small, i.e., when $\varepsilon^2 << 1$, a regular perturbation method can be used, namely the solution for the unknown field variables can be expanded as a power series in terms of ε^2:

$$X = X_0 + \varepsilon^2 X_2 + \varepsilon^4 X_4 + O(\varepsilon^6), \quad \varepsilon^2 << 1 \tag{8}$$

where $X = p,\ u_x,\ u_y$. Strictly, the perturbation theory implemented here is valid provided that $max_{0\le x^*\le \ell}(H^*(x^*) + \Phi^*(x^*))/\ell << 1$. Thus, henceforth we assume that the wall functions H^* and Φ^* are such that this requirement is fulfilled. Substituting Eq. (8) into Eqs. (2–7), expanding all quantities in terms of ε^2, and collecting the terms of the same order of magnitude with respect to ε^2, we derive the sequence of perturbation equations:

$$\frac{\partial u_{x,j}}{\partial x} + \frac{\partial u_{y,j}}{\partial y} = 0, \tag{9}$$

$$-\frac{\partial p_j}{\partial x} + \frac{\partial^2 u_{x,j-2}}{\partial x^2} + \frac{\partial^2 u_{x,j}}{\partial y^2} = 0, \tag{10}$$

$$-\frac{\partial p_j}{\partial y} + \frac{\partial^2 u_{y,j-4}}{\partial x^2} + \frac{\partial^2 u_{y,j-2}}{\partial y^2} = 0, \tag{11}$$

$$\frac{\partial^2 p_j}{\partial y^2} + \frac{\partial^2 p_{j-2}}{\partial x^2} = 0 \tag{12}$$

where $j = 0,2,4,6,\ldots$ and $u_{x,\,j} = u_{y,\,j} = p_j = 0$ for $j < 0$ have been introduced for completeness. The auxiliary conditions are:

$$u_{x,j} = u_{y,j} = 0 \quad \text{at } y = -\Phi(x) \text{ and } H(x), \quad -1 \le x \le 1, \tag{13}$$

$$\int_{-\Phi(x)}^{H(x)} u_{x,j}(x,y)dy = \delta_{0,j}. \tag{14}$$

In Eq. (14), the Kronecker delta, $\delta_{i,\,j} = 1(0)$ if $i = j$ (otherwise), has been used.

The solution procedure consists of the following steps:

(i) Integrate twice Eq. (12) with respect to y to find p_j in the general form $p_j = a_{j-2}(x,\ y) + \Pi_j(x)y + \hat{P}_j(x)$ where Π_j and $\hat{P}_j$ are unknown functions of x that must be determined, and $a_{j-2}(x,\ y)$ is the fully known part of the solution which results from the double integration of $-\partial^2 p_{j-2}/\partial x^2$ with respect to y.
(ii) Substitute p_j in Eq. (11) to find $\Pi_j(x)$.
(iii) Substitute p_j in Eq. (10) and integrate twice the resulting equation with respect to y and apply the no-slip conditions at both walls to find $u_{x,\,j}$.
(iv) Substitute $u_{x,\,j}$ in the integral constraint, Eq. (14), to find $\hat{P}'_j(x)$.

(v) Substitute $u_{x,j}$ in Eq. (9), integrate with respect to y, and apply the no-penetration boundary condition at the lower wall to find $u_{y,j} = -\int_{-\Phi(x)}^{y} \frac{\partial}{\partial x} u_{x,j}(x, s)ds$.

Note that the solution for $u_{y,j}$ satisfies the no-penetration condition at the upper wall, $u_{y,j}(x, H(x)) = 0$. Indeed, by evaluating the solution for $u_{y,j}$, found in step (v), at $y = H(x)$ and applying the Leibniz rule, gives:

$$u_{y,j}(x, H(x)) + \frac{d}{dx}\left(\int_{-\Phi(x)}^{H(x)} u_{x,j}(x, y)dy\right) - H'(x)u_{x,j}(x, H(x)) - \Phi'(x)u_{x,j}(x, -\Phi(x)) = 0 \tag{15}$$

where throughout the paper the primes denote derivatives with respect to the axial coordinate, x. Equation (15) reduces to $u_{y,j}(x, H(x)) = 0$ because the third and the fourth terms vanish owing to the no-slip condition given by Eq. (13), and the second term is zero, too, due to the integral constraint given by Eq. (14). Therefore, although the continuity equation used to determine $u_{y,j}$ is first order in y, the solution satisfies both boundary conditions for $u_{y,j}$ as previously reported in Ref. [34], too.

2.2 Solution

Following the procedure described in the previous Subsection, we find the analytical solution for the field variables up to fourth-order in ε, i.e., X_0, X_2, and X_4 where $X = p, u_x, u_y$. We mention that the zero- and second-order solutions given below fully agree with the analytical results derived by Hinojosa et al. [35] provided that the different scale for the pressure used by Hinojosa et al. [35] is taken into account. Also, for $\Phi(x) = 1/2$ our solution up to fourth-order fully matches the solution derived by Tavakol et al. [34] provided that first the transformations $\tilde{y} = y + 1/2$ and $\tilde{H} = H + 1/2$ are implemented (due to the fact that the origin of the coordinate system is placed in the midplane at the entrance of the channel and not at the lower wall as Tavakol et al. [34] did).

For convenience, we introduce the reduced y-coordinate $\hat{y} = (y + \Phi(x))\big/(H(x) + \Phi(x))$ so that $0 \le \hat{y} \le 1$, and we also omit the explicit dependence of the shape functions on the x-coordinate.

2.2.1 Zero-order solution

The zero-order solution corresponds to the classical lubrication theory, and is given as:

$$u_{x,0}(x, \hat{y}) = \frac{6\hat{y}(1-\hat{y})}{H + \Phi}, \quad u_{y,0}(x, \hat{y}) = \left(\hat{y}\, H' - (1-\hat{y})\, \Phi'\right)u_{x,0}(x, \hat{y}), \quad p_0(x) = p_0(1) + 12\int_x^1 \frac{ds}{(H(s) + \Phi(s))^3}. \tag{16}$$

In the above equation, $p_0(1)$ is arbitrary and can be considered zero without loss of generality. Its value does not affect the higher-order solutions which are shown below, nor it affects the required pressure drop needed to drive the flow.

2.2.2 Second-order solution

The second-order solution is found as follows:

$$\begin{aligned} u_{x,2}(x, \hat{y}) &= \frac{\hat{y}(1-\hat{y})}{H + \Phi}\left(\left(\hat{y} - \frac{1}{2}\right)a_1(x) + \left(\hat{y}^2 - \frac{3}{10}\right)a_2(x)\right), \\ u_{y,2}(x, \hat{y}) &= \left(H'\,\hat{y} - (1-\hat{y})\Phi'\right)u_{x,2}(x, \hat{y}) + \frac{\hat{y}^2(1-\hat{y})^2}{4}\left(a_1'(x) + \frac{(3+4\hat{y})a_2'(x)}{5}\right), \\ p_2(x, \hat{y}) &= \hat{P}_2(x) + \sum_{k=0}^{2} \hat{y}^k\, p_{2,k}(x). \end{aligned} \tag{17}$$

The functions that appear in $u_{x,2}$ are given by:

$$\begin{aligned} a_1(x) &= 24\Phi'\big(H'+\Phi'\big) - (H+\Phi)\big(H''+5\Phi''\big), \\ a_2(x) &= 3\Big(-4\big(H'+\Phi'\big)^2 + (H+\Phi)\big(H''+\Phi''\big)\Big). \end{aligned} \tag{18}$$

Also, the functions that appear in p_2 are:

$$p_{2,0}(x) = \frac{6\Phi^2\big(H'-\Phi'\big) - 12H\Phi\big(H'+2\Phi'\big)}{(H+\Phi)^4}, \quad p_{2,1}(x) = \frac{12\big(H'+2\Phi'\big)}{(H+\Phi)^2}, \quad p_{2,2}(x) = -\frac{18\big(H'+\Phi'\big)}{(H+\Phi)^2}. \tag{19}$$

Finally, the first derivative of $\hat{P}_2$ with respect to x is given by:

$$\begin{aligned} \frac{d\hat{P}_2}{dx} = \frac{6}{5(H+\Phi)^5}\big\{ & 6\big(4\Phi^2 - H^2 - 7H\Phi\big)H'^2 + 4\big(7H^2 - 16H\Phi + 7\Phi^2\big)H'\Phi' \\ & + 6\big(4H^2 - 7H\Phi - \Phi^2\big)\Phi'^2 - (H+\Phi)\big(H^2 - 8H\Phi + 6\Phi^2\big)H'' \\ & - (H+\Phi)\big(6H^2 - 8H\Phi + \Phi^2\big)\Phi''\big\}. \end{aligned} \tag{20}$$

2.2.3 Fourth-order solution

The fourth-order solution is found as:

$$\begin{aligned} u_{x,4}(x,\hat{y}) &= \frac{\hat{y}(1-\hat{y})}{H+\Phi}\left(\left(\hat{y}-\frac{1}{2}\right)A_1(x) + \left(\hat{y}^2-\frac{3}{10}\right)A_2(x) + \left(\hat{y}^3-\frac{1}{5}\right)A_3(x) + \left(\hat{y}^4-\frac{1}{7}\right)A_4(x)\right), \\ u_{y,4}(x,\hat{y}) &= \big(H'\,\hat{y} - (1-\hat{y})\Phi'\big)u_{x,4}(x,\hat{y}) \\ &\quad + \frac{\hat{y}^2(1-\hat{y})^2}{4}\left\{A_1' + \frac{\big(3+4\hat{y}\big)A_2'}{5} + \frac{2\big(3+4\hat{y}+5\hat{y}^2\big)A_3'}{15} + \frac{2\big(3+\hat{y}\big(4+\hat{y}\big(5+6\hat{y}\big)\big)\big)A_4'}{21}\right\}, \\ p_4(x,\hat{y}) &= \hat{P}_4(x) + \frac{1}{(H+\Phi)^2}\sum_{j=0}^{4}\hat{y}^j\,p_{4,j}(x) \end{aligned} \tag{21}$$

where functions $A_j = A_j(x)$, $j = 1, 2, 3, 4$ and $p_{4,j} = p_{4,j}(x)$, $j = 0, 1, 2, 3, 4$, are provided for convenience in the Appendix in terms of the shape functions $H = H(x)$ and $\Phi = \Phi(x)$ and their derivatives. The first derivative of $\hat{P}_4$ with respect to x is found as follows:

$$\begin{aligned} \frac{d\hat{P}_4}{dx} = {} & \frac{1}{G^3}\left(2G'p_{4,0} + \frac{G'+2H'}{2}p_{4,1} + \frac{G'+5H'}{5}p_{4,2} + \frac{G'+9H'}{10}p_{4,3} + \frac{2\big(G'+14H'\big)}{35}p_{4,4}\right) \\ & - \frac{1}{G^2}\left(p_{4,0}' + \frac{p_{4,1}'}{2} + \frac{3p_{4,2}'}{10} + \frac{p_{4,3}'}{5} + \frac{p_{4,4}'}{7}\right) + \frac{222G'^4}{175G^3} - \frac{24G'^3H'}{5G^3} - \frac{2G''^2}{35G} - \frac{2H''^2}{5G} - \frac{3G^{(4)}}{350} \\ & + \frac{2H'G^{(3)}}{5G} - \frac{4H'H^{(3)}}{5G} + G'^2\left(\frac{24H'^2}{5G^3} + \frac{506G''}{175G^2} - \frac{14H''}{5G^2}\right) + G''\left(\frac{24H'^2}{5G^2} + \frac{2H''}{5G}\right) \\ & + G'\left(-\frac{38H'G''}{5G^2} + \frac{28H'H''}{5G^2} - \frac{32G^{(3)}}{175G} + \frac{2H^{(3)}}{5G}\right) \end{aligned} \tag{22}$$

where $G \equiv H + \Phi$ has been used for convenience. Note that all the analytical solutions derived in this work have been checked for their correctness using the "Mathematica" symbolic software [46].

2.3 Pressure drop

The most interesting quantity for this type of flow is the required pressure drop to maintain the constant flowrate in the channel. First, however, we define the average of any dependent variable, $f = f(x, y)$, at a cross section from the inlet plane, i.e.,

$$\overline{f}(x) := \int_{-\Phi(x)}^{H(x)} f(x,y)dy \Big/ \int_{-\Phi(x)}^{H(x)} dx = \int_0^1 f(x, -\Phi(x) + \hat{y}(\Phi(x) + H(x)))\, d\hat{y} \tag{23}$$

where in the second equality the reduced y-coordinate has been used. We also define the difference operator, Δ, for any dependent flow variable, $f = f(x, y)$, as $\Delta f := f(x = 0, y) - f(x = 1, y)$. Therefore, the average pressure drop is given as $\Delta\overline{p} \equiv \overline{p}(0) - \overline{p}(1)$, where $\overline{p}(0) = \int_0^1 p(0, \hat{y})\, d\hat{y}$ and $\overline{p}(1) = \int_0^1 p(1, \hat{y})\, d\hat{y}$; note that $p(0, \hat{y})$, $p(1, \hat{y})$ have been used for brevity instead of $p(0, -\Phi(0) + \hat{y}(\Phi(0) + H(0)))$, $p(1, -\Phi(1) + \hat{y}(\Phi(1) + H(1)))$,respectively. Hence, based on the perturbation expansion up to $O(\varepsilon^4)$, the average pressure drop is $\Delta\overline{p} \approx \Delta\overline{p}_0 + \varepsilon^2\Delta\overline{p}_2 + \varepsilon^4\Delta\overline{p}_4$. Recalling that $p_0 = p_0(x)$, the individual components are:

$$\Delta\overline{p}_0 = \int_0^1 p_0(0)d\hat{y} - \int_0^1 p_0(1)d\hat{y} = p_0(0) - p_0(1) = -\int_0^1 \frac{dp_0}{dx}dx = 12\int_0^1 \frac{dx}{(H(x) + \Phi(x))^3}, \tag{24.1}$$

$$\Delta\overline{p}_2 = \int_0^1 p_2(0, \hat{y})d\hat{y} - \int_0^1 p_2(1, \hat{y})d\hat{y} = -\int_0^1 \frac{d\hat{P}_2}{dx}dx + \sum_{k=0}^{2} \frac{\Delta p_{2,k}}{k+1}, \tag{24.2}$$

$$\Delta\overline{p}_4 = \int_0^1 p_4(0, \hat{y})d\hat{y} - \int_0^1 p_4(1, \hat{y})d\hat{y} = -\int_0^1 \frac{d\hat{P}_4}{dx}dx + \sum_{k=0}^{4} \frac{\Delta p_{4,k}}{k+1}. \tag{24.3}$$

In Eqs. (24.2) and (24.3), $\hat{P}_2'(x)$ and $\hat{P}_4'(x)$ are given by Eqs. (20) and (22), respectively. Notice that the average pressure drop at $O(\varepsilon^2)$ and $O(\varepsilon^4)$ is not found by integrating only $-\hat{P}_2'(x)$ and $-\hat{P}_4'(x)$ along the$x$-direction, respectively, but additional correction terms appear, as these can be seen on the right-hand-side in Eqs. (24.2, 3). For periodic shape functions, the additional terms vanish, but this does not hold in general. For instance, even fully symmetric linearly contracting/expanding channels exhibit a nonzero first derivative at the inlet ($z = 0$) and outlet planes ($z = 1$), and therefore the additional terms at the right-hand-side of Eqs. (24.2, 3) contribute to the average pressure drop.

3 Flow in a tube

We consider the isothermal and incompressible steady axisymmetric flow of a simple Newtonian fluid in a tube with varying cross section, namely the radius of the tube changes with the distance from the inlet cross section. The length of the tube is ℓ, and the radius of the inlet cross section is h_0. We use a cylindrical coordinate system $r^*\theta^*z^*$ to describe the flow field, where z^* is the main flow direction, r^* is the radial, and θ^* is the azimuthal angle. The origin of the coordinate system is located at the axis of symmetry of the tube and at the inlet plane as shown in Fig. 1b. The wall of the tube is described by the shape function $H^* = H^*(z^*)$, with $H^*(z^* = 0) = h_0$, and hence the equation that describes the wall is $F^*(r^*, z^*) = r^* - H^*(z^*) = 0$. Obviously, the flow throughout the tube is allowed provided that $H^*(z^*) > 0$ for $z^* \in [0, \ \ell]$.The velocity vector in the flow domain is denoted by $\mathbf{u}^* = u_r^*\mathbf{e}_r + u_z^*\mathbf{e}_z$ ($\mathbf{e}_r$, $\mathbf{e}_z$ are the unit vectors along the r^*, z^* directions, respectively) and the total pressure by p^*; the latter is induced by the imposed flow-rate q at the inlet cross section, $q = 2\pi\int_0^{h_0} u_z(r^*, 0)\, r^*\, dr^*$.

Using the same assumptions as for the channel flow, the fluid motion in the tube is governed by Eq. (1), the domain of definition of which is $\Omega_{cyl} = \{(r^*, \theta^*, z^*)|0 < r^* < H^*(z^*),\ 0 \le \theta^* < 2\pi,\ 0 < z^* < \ell\}$. Note, however, that due to the symmetry with respect to the z^*-axis, $\partial/\partial\theta^* = 0$, and thus all the field variables are independent of θ^*. Equation (1) is accompanied with the usual no-slip and no-penetration boundary conditions along the wall, $\mathbf{u}^* = \mathbf{0}$ at $r^* = H^*(z^*)$, the symmetry conditions along the z^*-axis, $u_r^* = \partial u_z^*/\partial r^* = 0$ at $r^* = 0$, and the integral constraint, $q = 2\pi\int_0^{H^*(z^*)} u_z(r^*, z^*)\, r^*\, dr^*$.

As for the channel flow, we introduce dimensionless variables based on the lubrication theory, i.e., $X = X^*/X_c$ where $X = r,\ z,\ u_r,\ u_z,\ p,\ H$, and X_c is the relevant characteristic scale for X^*. The z^*-coordinate is scaled by ℓ and the r^*-coordinate by h_0, while the angle θ^* is already dimensionless. The radius of the inlet cross section, h_0, is also used to make dimensionless the shape function H^*. From the mass flow-rate at the inlet cross section we find that the characteristic scale for u_z^* is $q/(2\pi h_0^2)$. Next, with the aid of the continuity equation, we find that the characteristic scale for u_r^* is $q/(2\pi h_0 \ell)$. Last, from the component of the momentum balance along the axial direction, we determine the characteristic scale for the pressure, $\mu\, q\, \ell/(2\pi h_0^4)$. Thus, the final scalar dimensionless governing equations are:

$$\frac{\partial}{\partial z}(r\,u_z) + \frac{\partial}{\partial r}(r\,u_r) = 0, \tag{25}$$

$$-\frac{\partial p}{\partial z} + \varepsilon^2 \frac{\partial^2 u_z}{\partial z^2} + \frac{1}{r}\frac{\partial}{\partial r}\left(r\frac{\partial u_z}{\partial r}\right) = 0, \tag{26}$$

$$-\frac{\partial p}{\partial r} + \varepsilon^4 \frac{\partial^2 u_r}{\partial z^2} + \varepsilon^2 \frac{\partial}{\partial r}\left(\frac{1}{r}\frac{\partial}{\partial r}(r\,u_r)\right) = 0, \tag{27}$$

$$\frac{1}{r}\frac{\partial}{\partial r}\left(r\frac{\partial p}{\partial r}\right) + \varepsilon^2 \frac{\partial^2 p}{\partial z^2} = 0 \tag{28}$$

where $\varepsilon \equiv h_0/\ell$ is the aspect ratio of the tube (recall that $h_0 = H^*(0)$). The auxiliary conditions (boundary, symmetry, and integral conditions) are:

$$u_r = u_z = 0 \quad \text{at } r = H(z),\ 0 \le z \le 1, \tag{29}$$

$$u_r = \frac{\partial u_z}{\partial r} = 0 \quad \text{at } r = 0,\ 0 \le z \le 1, \tag{30}$$

$$\int_0^{H(z)} u_z(r,z)\, r\, dr = 1. \tag{31}$$

Equation (31) results from the integration of Eq. (25) along the radial direction between the limits $r = 0$ and $r = H(z)$, applying the no-penetration boundary condition, Eq. (29), and using the dimensionless flow-rate at the inlet, $\int_0^1 u_z(r,\,0)\, r\, dr = 1$, where, due to the characteristic scales used, $H(0) = 1$. The shape function H is considered known in advance; for $H(z) = 1$ one gets a straight tube.

3.1 Method of solution and solution procedure

When the aspect ratio of the tube, ε, is small, a regular perturbation method can be used, namely the solution for the unknown field variables, $p,\ u_r,\ u_z$, can be expanded as a power series in terms of ε^2 as shown in Eq. (8). As we mentioned before for the channel flow, the main requirement for our analysis to be valid is the magnitude of the ratio $max_{0\le x^*\le \ell}\, H^*(x^*)/\ell$ to be much less than unity. Thus, henceforth we assume that the wall function H^* is such that this requirement is fulfilled. Following the same procedure as for the channel flow, and introducing $u_{r,\,j} = u_{z,\,j} = p_j = 0$ for any $j < 0$ for completeness, we derive the sequence of perturbation equations:

$$\frac{\partial}{\partial z}(r\,u_{z,j}) + \frac{\partial}{\partial r}(r\,u_{r,j}) = 0, \tag{32}$$

$$-\frac{\partial p_j}{\partial z} + \frac{\partial^2 u_{z,j-2}}{\partial z^2} + \frac{1}{r}\frac{\partial}{\partial r}\left(r\frac{\partial u_{z,j}}{\partial r}\right) = 0, \tag{33}$$

$$-\frac{\partial p_j}{\partial r} + \frac{\partial^2 u_{r,j-4}}{\partial z^2} + \frac{\partial}{\partial r}\left(\frac{1}{r}\frac{\partial}{\partial r}(r\,u_{r,j-2})\right) = 0, \tag{34}$$

$$\frac{\partial}{\partial r}\left(r\frac{\partial p_j}{\partial r}\right) + \frac{\partial^2}{\partial z^2}(r\,p_{j-2}) = 0 \tag{35}$$

where $j = 0,\ 2,\ 4,\ \ldots$ The accompanying auxiliary conditions are:

$$u_{r,j} = u_{z,j} = 0 \quad \text{at } r = H(z),\ 0 \le z \le 1, \tag{36}$$

$$u_{r,j} = \frac{\partial u_{z,j}}{\partial r} = 0 \quad \text{at } r = 0,\ 0 \le z \le 1, \tag{37}$$

$$\int_0^{H(z)} u_{z,j}(r,z)\, r\, dr = \delta_{0,j}. \tag{38}$$

The solution procedure is like that described for the channel flow:

(i) Integrate twice Eq. (35) with respect to r to find the general solution for p_j:

$$p_j = \underbrace{-\int \left(\frac{1}{r} \int \frac{\partial^2}{\partial z^2}(r\, p_{j-2}) dr \right) dr}_{a_{j-2}(r,z)} + \hat{P}_j(z) \tag{39}$$

where the condition $\left| p_j(0,\, z) \right| < \infty$ has been used, and $\hat{P}_j = \hat{P}_j(z)$ is an unknown function that must be determined.

(ii) Substitute Eq. (39) into Eq. (33) and integrate twice with respect to r to obtain $u_{z,\,j}$:

$$u_{z,j} = \frac{\hat{P}_j'(z)}{4}\left(r^2 - H^2\right) + \underbrace{\int_r^{H(z)} \left(\frac{1}{s} \int \frac{\partial^2}{\partial z^2}(s u_{z,j-2}(s,z)) - \frac{\partial}{\partial z}(s a_{j-2}(s,z)) \right) ds \right) ds}_{\beta_{j-2}(r,z)} \tag{40}$$

where the no-slip condition, $u_{z,\,j}(H(z),\, z) = 0$, and the symmetry condition, $\partial u_{z,\,j} \big/ \partial r = 0$ at $r = 0$, have been applied.

(iii) Substitute $u_{z,\,j}$ in the integral constraint, Eq. (38), to determine $\hat{P}_j'(z)$:

$$\hat{P}_j'(z) = \frac{16}{H^4}\left(-\delta_{0,j} + \int_0^{H(z)} \beta_{j-2}(r,z)\, r\, dr \right). \tag{41}$$

(iv) Substitute $u_{z,\,j}$ in Eq. (32), integrate with respect to r, and apply the symmetry condition $u_{r,\,j}(r = 0,\, z) = 0$ to find $u_{r,\,j}$:

$$u_{r,j} = -\frac{1}{r} \int_0^r \frac{\partial}{\partial z}(s\, u_{z,j}(s,z)) ds. \tag{42}$$

Next, we check the no-penetration condition at the upper wall, $u_{r,\,j}(H(z),\, z) = 0$. Evaluating Eq. (42) at $r = H(z)$ and applying the Leibniz rule gives:

$$u_{r,j}(H(z),z)\, H(z) + \frac{d}{dz}\left(\int_0^{H(z)} u_{z,j}(r,z)\, r\, dr \right) - H'(z) u_{z,j}(H(z),z) = 0. \tag{43}$$

The third term vanishes owing to the no-slip condition given by Eq. (13), and the second term is zero, too, due to integral constraint given by Eq. (38). Therefore, Eq. (43) simply reduces to $u_{r,\,j}(H(z),\, z) = 0$. This shows that albeit the continuity equation used to determine $u_{r,\,j}$ is first order in r, both the symmetry and the no-penetration conditions are satisfied.

Finally, we confirm that the solution for p_j, $u_{r,\,j-4}$ and $u_{r,\,j-2}$ satisfies Eq. (34). This completes the solution of the equations at order $O(\varepsilon^j)$, $j = 0,2,4,\ldots$

3.2 Solution

Following the procedure describe in the previous Subsection, we find the analytical solution for the field variables up to forth-order in ε, i.e., the quantities X_0, X_2, and X_4 where $X = p, u_r, u_z$. For convenience, we define the reduced radial coordinate $\hat{r} = r/H(z)$ so that $0 \le \hat{r} \le 1$, which helps us to produce more compact expressions for the solutions, and for further simplicity we omit the explicit dependence of the shape function on the axial coordinate.

3.2.1 Zero-order solution

The zero-order solution corresponds to the classical lubrication theory, and is given as:

$$u_{z,0}(\hat{r},z) = 4(1-\hat{r}^2)/H^2, \quad u_{r,0}(\hat{r},z) = \hat{r}\,H'\,u_{z,0}(\hat{r},z), \quad p_0(z) = \hat{P}_0, \quad \hat{P}_0'(z) = -16/H^4, \tag{44}$$

The last expression in Eq. (44) can be used to determine the pressure distribution, up to a constant, along the tube:

$$p_0(z) = p_0(1) - \int_z^1 \hat{P}'_0(s)ds = p_0(1) + 16\int_z^1 H^{-4}(s)ds. \tag{45}$$

Note, however, that only the quantity $\hat{P}_0'(z)$ really matters for the calculation of the higher-order solutions and the required pressure drop (see the next Subsection).

3.2.2 Second-order solution

The second-order solution is found as follows:

$$\begin{aligned} u_{z,2}(\hat{r},z) &= \frac{2}{3}(1-\hat{r}^2)(1-3\hat{r}^2)\left(\frac{5H'^2}{H^2} - \frac{H''}{H}\right), \\ u_{r,2}(\hat{r},z) &= \hat{r}H'u_{z,2}(\hat{r},z) - \frac{\hat{r}(1-\hat{r}^2)^2(5H'^2 - HH'')'}{3H}, \\ p_2(\hat{r},z) &= \hat{P}_2(z) - \frac{16H'}{H^3}\hat{r}^2 \end{aligned} \tag{46}$$

where

$$\hat{P}_2'(z) = \frac{8H''}{3H^3} - \frac{88H'^2}{3H^4}. \tag{47}$$

3.2.3 Fourth-order solution

The fourth-order solution is found as follows:

$$\begin{aligned} u_{z,4}(\hat{r},z) = (1-\hat{r}^2)\Bigg(&\frac{5(-1-60\hat{r}^2+126\hat{r}^4)H'^4}{36H^2} - \frac{5(7-48\hat{r}^2+54\hat{r}^4)H'^2H''}{18H} \\ &+ \frac{(8-39\hat{r}^2+30\hat{r}^4)}{18}H'H''' + \frac{1}{72}\Big((32-141\hat{r}^2+90\hat{r}^4)H''^2 + (-2+9\hat{r}^2-6\hat{r}^4)HH^{(4)}\Big)\Bigg), \end{aligned} \tag{48.1}$$

$$u_{r,4}(\hat{r},z) = \hat{r}H'u_{z,4}(\hat{r},z) - \frac{\hat{r}(1-\hat{r}^2)^2(5H'^2 - HH'')'}{3H}, \tag{48.2}$$

$$p_4(\hat{r},z) = \hat{P}_4 - \frac{H^2\hat{P}_2''}{4}\hat{r}^2 + H^4\left(\frac{H'}{H^5}\right)''\hat{r}^4 \tag{48.3}$$

where

$$\hat{P}_4'(z) = \frac{238H'^2H''}{9H^3} - \frac{115H'^4}{9H^4} - \frac{41H''^2}{18H^2} - \frac{22H'H^{(3)}}{9H^2} - \frac{H^{(4)}}{18H}. \tag{49}$$

3.3 Pressure drop

The required average pressure drop to maintain the constant flowrate in the tube is found as follows. First, the average of any dependent variable, $f = f(r, z)$, at a cross section from the inlet plane is defined as

$$\overline{f}(z) := \int_0^{H(z)} f(r,z) r dr \Big/ \int_0^{H(z)} r dr = 2 \int_0^1 f\big(\hat{r} H(z), z\big) \hat{r} d\hat{r} \tag{50}$$

where the integration along the polar angle θ has been ignored due to the axisymmetry of the geometry and the flow field, and in the second equality the reduced radial coordinate, $\hat{r}$, has been used. Also, we define the difference operator $\Delta f := f(z = 0) - f(z = 1)$ of any dependent variable $f = f(r, z)$, and thus the average pressure drop is given as $\Delta\overline{p} \equiv \overline{p}(0) - \overline{p}(1)$, where $\overline{p}(0) = 2\int_0^1 p(\hat{r}\, H(0), 0)\, \hat{r}\, d\hat{r}$ and $\overline{p}(1) = 2\int_0^1 p(\hat{r}\, H(1), 1)\, \hat{r}\, d\hat{r}$. Finally, based on the perturbation expansion up to $O(\varepsilon^4)$, the average pressure drop is $\Delta\overline{p} \approx \Delta\overline{p}_0 + \varepsilon^2 \Delta\overline{p}_2 + \varepsilon^4 \Delta\overline{p}_4$. The individual components are found as:

$$\Delta\overline{p}_0 = 2\int_0^1 p_0(\hat{r}H(0),0)\hat{r}d\hat{r} - 2\int_0^1 p_0(\hat{r}H(1),1)\hat{r}d\hat{r} = -\int_0^1 \hat{P}_0'(z)dz = 16\int_0^1 H^{-4}(z)dz, \tag{51.1}$$

$$\Delta\overline{p}_2 = 2\int_0^1 p_2\big(\hat{r}H(0),0\big)\hat{r}d\hat{r} - 2\int_0^1 p_2\big(\hat{r}H(1),1\big)\hat{r}d\hat{r} = -\int_0^1 \hat{P}_2'(z)dz + \Delta\left(-8\frac{H'}{H^3}\right), \tag{51.2}$$

$$\Delta\overline{p}_4 = 2\int_0^1 p_4\big(\hat{r}H(0),0\big)\hat{r}d\hat{r} - 2\int_0^1 p_4\big(\hat{r}H(1),1\big)\hat{r}d\hat{r} = -\int_0^1 \hat{P}_4'(z)dz + \Delta\left(\frac{H^4(H'/H^5)''}{3} - \frac{H^2\hat{P}_2''}{8}\right). \tag{51.3}$$

In Eqs. (51.2, 3), $\hat{P}_2'(z)$ and $\hat{P}_4'(z)$ are given by Eqs. (47) and (49), respectively. As for the channel flow, we notice that the average pressure drop at $O(\varepsilon^2)$ and $O(\varepsilon^2)$ is not found only by integrating $-\hat{P}_2'(z)$ and $-\hat{P}_4'(z)$ along the$z$-direction, but additional terms appear, as these can be seen on the right-hand-side in Eqs. (51.2) and (51.3). For fully periodic tubes, the additional terms vanish, however this does not hold in general. For instance, even linearly contracting/expanding channels exhibit a nonzero first derivative at the inlet ($z = 0$) and outlet cross section ($z = 1$), i.e., $H'(0) \neq 0$ and $H'(1) \neq 0$, and therefore the additional terms in Eqs. 51.2, 51.3) contribute to the average pressure drop.

4 Results and discussion

We proceed by presenting results for the average pressure drop required to maintain the constant flowrate through the channel or tube using specific examples for the shape function(s). We are interested most in configurations with multiple constrictions, converging or diverging channels/tubes, and wavy and undulating or rough channels/tubes with relatively large wavenumber and small amplitude; a few examples are shown in Fig. 2. For all the selected cases, the integrations needed in Eqs. (24.1–3) and Eqs. (51.1–3) are performed analytically, yielding the average pressure drop explicitly in terms of the parameters entering into the shape function(s). More complex configurations can be easily considered, however, the integrations in Eqs. (24.1–3) and Eqs. (51.1–3) must then be performed numerically.

Since the main purpose of the current work is the derivation of more accurate expressions for the average pressure drop compared to the classical leading-order lubrication approximation, we also investigate techniques that increase the accuracy of the obtained truncated perturbation solutions. This issue has been discussed recently in the literature due to the availability of high-order solutions obtained with the aid of symbolic computer software (such as the "Mathematica" software used here [46]). It has also been reported that when many terms (three, at least) in a perturbation series are known, techniques that increase their accuracy and extend their domain of convergence can be applied [47]. For fundamental nonlinear viscoelastic flow problems, three techniques have been studied extensively and checked for their accuracy and efficiency [48]. These are Euler's linear transformation (when the series is alternating), the nonlinear Shanks transformation [49, 50],

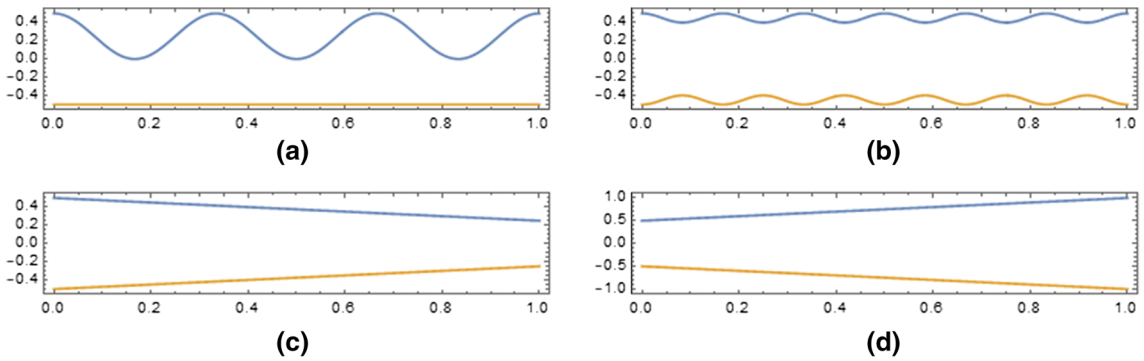

Fig. 2 Typical configurations with aspect ratio $\varepsilon = 1/4$ (**a**) Asymmetric channel with a flat boundary and multiple constrictions (three) imposed by the upper boundary, (**b**) Symmetric wavy/rough channel with many oscillations (six) and low amplitude (0.1), (**c**) Symmetric and converging channel with $h_f = 1/4$, (**d**) Symmetric and expanding channel with $h_f = 1$

and the Padé-type approximants [51]. The techniques have also been applied successfully to a variety of viscoelastic flows around cylinders and spheres yielding accurate formulas for the drag force on the cylinder or sphere [52–56]. Here, the diagonal [2/2] Padé-approximant and the Shanks transformation are applied to the three-term series for the average pressure drop, which based on the perturbation scheme is given as $\Delta\overline{p} \approx \Delta\overline{p}_0+\varepsilon^2\Delta\overline{p}_2^2+\varepsilon^4\Delta\overline{p}_4$. In this case, both Shanks transformation and the diagonal [2/2] Padé-approximant produce the same transformed expression for Δp, denoted with the subscript "S":

$$\Delta\overline{p}_S = \Delta\overline{p}_0 + \frac{\varepsilon^2\Delta\overline{p}_2^2}{\Delta\overline{p}_2 - \varepsilon^2\Delta\overline{p}_4}. \tag{52}$$

By construction, Eq. (52) agrees well with the original three-term solution for small values of ε. Thus, for the range of parameters for which Eq. (52) agrees with the original solution, one is confident that high accuracy of the results has been achieved. Furthermore, and based on the experience regarding the performance of the transformed formula(s) in many fluid mechanics problems, Eq. (52) is expected to be accurate for an extended range of parameters; this range however cannot be determined a-priori. Hereafter, we will be referring to Eq. (52) as the "acceleration formula", and we also emphasize that in general there is no formal proof about the superiority of Eq. (52) versus the truncated original perturbation series. Thus, Eq. (52) should be used with appropriate caution. For instance, we mention the case where $\Delta\overline{p}_2$ and $\Delta\overline{p}_4$ have the same sign, and thus Eq. (52) becomes singular at a critical aspect ratio $\varepsilon_c = \pm\sqrt{\Delta\overline{p}_2/\Delta\overline{p}_4}$, a situation that was not encountered for the specific examples studied in the subsequent Sections.

To summarize, the truncated original perturbation series for the average pressure drop is given by the three-term expression $\Delta\overline{p} \approx \Delta\overline{p}_0 + \varepsilon^2\Delta\overline{p}_2^2 + \varepsilon^4\Delta\overline{p}_4$, and its transformed expression by Eq. (52). In the window of parameters for which the two expressions agree well, high accuracy and convergence of the results is indicated. In addition, Eq. (52) is expected to be more accurate than the original solution, and therefore it can be trusted, for an extended set of parameter values.

4.1 Flow in a channel

First, we present the results for the confined flow in an asymmetric channel the lower wall of which is flat, $\Phi(x) = 1/2$, while the upper wall is described by the shape function $H(x) = \frac{1}{2}(1 - \lambda(1 - \cos(2m\pi x)))$,i.e., multiple constrictions, m, of the same amplitude, λ, (for simplicity) are considered, where $m = 1, 2, 3, \ldots$ and $0 \le \lambda < 1$. Thus, for any $x \in [0, 1]$, $0 < H(x) + \Phi(x) \le 1$, where $H(x) + \Phi(x) = 0$ can be attained only when $\lambda = 1$. For $m = 1$, this case corresponds to the main case presented by Tavakol et al. [34]; note that in Ref. [34] the authors use the aspect ratio $\delta \equiv h_0/(\ell/2) = 2h_0/\ell = 2\varepsilon$, the x-axis varies from -1 to 1, and that the origin of their coordinate system is located at the lower wall and in the middle of the channel (see Fig. 1 in Ref. [34]). Defining the shape functions as mentioned above, Eqs. (24.1-3) can be calculated analytically to give the average pressure drop in the channel:

$$\Delta\overline{p} \approx \frac{3\left(8 - 8\lambda + 3\lambda^2\right)}{2(1-\lambda)^{5/2}} + \frac{6\lambda^2}{5(1-\lambda)^{3/2}}\chi^2 + \frac{4\left(428\left(-1+\sqrt{1-\lambda}\right) + 214\left(2-\sqrt{1-\lambda}\right)\lambda - 53\lambda^2\right)}{175\sqrt{1-\lambda}}\chi^4 \tag{53}$$

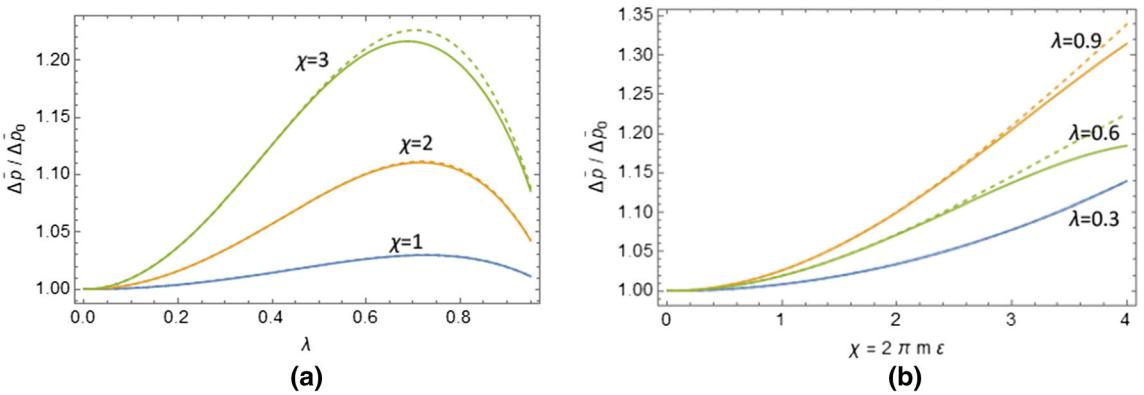

Fig. 3 The reduced average pressure drop for an asymmetric channel with a flat lower wall and a varying upper wall with multiple constrictions (**a**) as function of the amplitude of the constriction for $\chi = 1$, 2, and 3 where $\chi = 2\ \pi\ \mathrm{m}\ \varepsilon$; (**b**) as function of χ for $\lambda = 0.3$, 0.6, and 0.9. The corresponding results obtained using the acceleration formula, Eq. (52), are also shown with dashed lines for comparison

where the modified aspect ratio $\chi \equiv 2\pi m\,\varepsilon$ has been used. As expected, for $\lambda \to 1^-$ the upper wall touches the lower wall, and the fluid cannot continue to flow leading to a blow-up of $\Delta\overline{p}$. For $m = 1$ Eq. (53) fully agrees with the corresponding expression derived in Ref. [34] if the difference in the domain along the x-direction and the different definition of the aspect ratio are taken into account; note also that in Ref. [34] the results have been presented up to $\delta = 1$ which corresponds to $\varepsilon = 0.5$. We reiterate that Eq. (53) is valid for multiple constrictions (i.e., for $m > 1$) asymptotically as $\varepsilon \to 0^+$ provided that $\left|\Delta\overline{p}_0\right| >> \varepsilon^2\left|\Delta\overline{p}_2\right| >> \varepsilon^4\left|\Delta\overline{p}_4\right|$. In order to focus on the effect of the higher-order terms, namely on the effect of a non-vanishing aspect ratio, we show in Fig. 3a the reduced average pressure drop, $\Delta\overline{p}/\Delta\overline{p}_0$, as function of the amplitude of the constriction(s), λ, for $\chi = 1,\ 2,$ and 3. Also, in Fig. 3b, we show $\Delta\overline{p}/\Delta\overline{p}_0$ as function of the modified aspect ratio χ, for $\lambda = 0.3$, 0.6, and 0.9. The corresponding results for $\Delta\overline{p}_S/\Delta\overline{p}_0$ according to the acceleration formula, Eq. (52), are also presented with dashed lines for comparison.

First, it is seen that for fixed χ and in the range $0 < \lambda \leq 0.9$ the required pressure drop is always above unity. Also, a global maximum which grows as the modified aspect ratio increases is observed at a critical amplitude of the constriction(s), λ_c. Notice that λ_c depends weakly on χ; for $\chi = 1,\ 2,$ and 3 the maximum is attained at $\lambda_c \approx 0.727,\ 0.716,$ and 0.688, respectively. Second, it is seen in Fig. 3b that for fixed λ the reduced average pressure drop increases monotonically with the increase in the modified aspect ratio, with the rate of increase being larger as the amplitude of the constriction(s) becomes higher. Finally, in both Figs. 3a and 3b, one can see clearly that the acceleration formula gives almost the same results with the original perturbation solution, with some minor differences observed only for large values of λ and χ. This is an indication for the high accuracy and convergence of the results, at least for $\lambda \lesssim \lambda_c$ and for the range of parameters investigated here, while the accuracy and convergence of the results for $\lambda \gtrsim \lambda_c$ require further investigations to be performed.

We proceed by investigating a symmetric wavy channel, namely both walls are described by the same shape function $\Phi(x) = H(x) = \frac{1}{2}\left(1 - \frac{\lambda}{2}(1 - \cos(2m\pi x))\right)$, $m = 1,\ 2,\ 3,\ \ldots$. Due to the requirement $\Phi(x) + H(x) = 2H(x) > 0$ for any $x \in [0,\ 1]$, the amplitude of the constriction(s) is restricted in the window $0 < \lambda < 1$; for $\lambda = 0$ one gets a straight channel with two parallel walls, while for $\lambda \to 1^-$ the upper wall reaches the lower wall and the flow is interrupted, i.e., a singularity is expected. Using these shape functions, Eq. (24.1-3) gives the average pressure drop in the channel:

$$\Delta\overline{p} \approx \frac{3\left(8 - 8\lambda + 3\lambda^2\right)}{2(1-\lambda)^{5/2}} + \frac{9\lambda^2}{5(1-\lambda)^{3/2}}\chi^2 + \frac{3\left(1928\left(-1+\sqrt{1-\lambda}\right) + 964\left(2-\sqrt{1-\lambda}\right)\lambda - 243\lambda^2\right)}{350\sqrt{1-\lambda}}\chi^4 \tag{54}$$

where the modified aspect ratio $\chi \equiv \pi m\,\varepsilon$ has been used. Interestingly, Eq. (54) is very similar to Eq. (53); the leading-order terms in these equations coincide (due to the fact that the quantity $\Phi + H$ is the same) but differences appear at the higher-order terms. Thus, the classical lubrication theory gives the same $\Delta\overline{p}_0$ for an asymmetric channel consisting of a flat and a varying wall, as described at the beginning of this Subsection, with a symmetric channel with two varying walls. On the contrary, the higher-order lubrication theory provides different solutions (as it should be expected). Equation (54) also shows that the average pressure drop becomes

Table 1 The dimensionless resistance to the flow, $f\mathrm{Re}$, as calculated in Ref. [57] using spectral methods and Richardson extrapolation, compared to the leading-order lubrication approximation (3rd column), to the analytical results from Eq. (54) (4th column), and to the transformed expression based on Eq. (52) (5th column)

Parameters	$f\mathrm{Re}$	$m\,(1-\lambda/2)^3\Delta\overline{p}_0$	$m\,(1-\lambda/2)^3\Delta\overline{p}$	$m\,(1-\lambda/2)^3\Delta\overline{p}_S$
$\alpha=0.07,\ R/L=0.16$	12.21354	12.178	12.2136	12.2136
$\alpha=0.10,\ R/L=0.16$	12.43974	12.3669	12.4398	12.4398
$\alpha=0.15,\ R/L=0.16$	13.0119	12.8454	13.0121	13.0122
$\alpha=0.20,\ R/L=0.50$	16.0*	13.5551	15.969	16.0709

*Indicates an approximate value extracted virtually from a figure in Ref. [57]

singular in the limit $\lambda \to 1^-$ as the gap vanishes. Finally, we mention that the results for $\Delta\overline{p}/\Delta\overline{p}_0$(and for $\Delta\overline{p}_S/\Delta\overline{p}_0$) follow the same general trends as those observed before for the asymmetric channel and thus are not shown here.

For $\lambda < 0$ Eq. (54) can be used to study an undulating symmetric channel, and to compare with high accuracy numerical solutions from the literature. In particular, Beris et al. [57] performed numerical spectral calculations of viscoelastic flows in a fully periodic, along the main flow direction, undulating channel. Denoting the average half-gap height of an equivalent straight channel by R, the wavelength of the undulation by L, and the amplitude of the undulation by αR, where α is dimensionless, the shape function for both the upper and the lower walls of the channel was $r_w^*(x^*) = R(1-\alpha\cos(2\pi x^*/L)), 0 \le x^* \le L$. Comparing r_w^* with the shape function used in the previous paragraph, i.e.,$H^*(x^*) = (h_0/2)(1-(\lambda/2)(1-\cos(2m\pi x^*/\ell)))$ (dimensional), one can confirm that the two formulations are equivalent provided that $\ell/m = L$, $\lambda = 2a/(a-1)$ and $m\,\varepsilon = 2(R/L)(1-\alpha)$. Since the calculations in Ref. [57] were performed in a computational cell of length L, in our comparison we set $m=1$. Thus, by defining a and R/L (i.e., the two dimensionless parameters that characterize the geometry) we can calculate λ and ε.

In Table 1, we compare the macroscopic dimensionless resistance of the flow, $f\mathrm{Re} \equiv 8\ \Delta p^* R^3/(\eta\ q\ L)$, obtained numerically in Ref. [57] with the analytical results for $\Delta\overline{p}$ given by Eq. (54). Taking into account the expressions between $\{\lambda,\ \varepsilon,\ m\}$ and $\{a,\ R/L\}$, one finds that $f\mathrm{Re} = m\ (1-\lambda/2)^3\Delta\overline{p}$. We were able to extract numerical results from Ref. [57] that correspond to four different geometries; the parameters are shown in the first column in the Table. The numerical values for $f\mathrm{Re}$, obtained with Richardson extrapolation, are shown along with the leading-order lubrication results, the high-order results (Eq. (54)) and the corresponding results obtained with the acceleration formula (Eq. (52)). In all cases, it is seen that the correction to the classical lubrication solution is significant, and, most importantly, that the higher-order lubrication theory agrees very well with the numerical results. It is also very interesting that the quality of the agreement remains approximately the same, even when α increases to 0.2. As far as the acceleration formula is concerned, its effect is inconsequential indicating that the original truncated perturbation solution as given by Eq. (54) has already converged.

Last, we investigate a symmetric contracting/expanding channel whose walls are described by the linear shape functions $\Phi(x) = H(x) = \frac{1}{2} + \left(h_f - \frac{1}{2}\right)x$ where $h_f > 0$ is the half-distance between the two walls at the exit plane. In this case, Eqs. (24.1–3) give:

$$\frac{\Delta\overline{p}}{\Delta\overline{p}_0} \approx 1 + \frac{1}{10}\chi^2 - \frac{17}{2800}\chi^4, \quad \Delta\overline{p}_0 = \frac{3(1+2h_f)}{2h_f^2}, \quad \chi \equiv (1-2h_f)\varepsilon. \tag{55}$$

Since only even powers of the modified aspect ratio χ appear in Eq. (55), its sign does not matter. Thus, Eq. (55) predicts the same result for converging ($0 < h_f < 1/2$) and diverging ($h_f > 1/2$) channels provided that $|\chi|$ is the same. This is a consequence of the linearity of the Stokes equations, Eqs. (2–5), and the fact that the converging and diverging channels are two mirror-image configurations of the sameshaped body (see also the discussion in Chapter 7 in Ref. [2]). For $\chi = 0$ (i.e., for $h_f = 1/2$) one gets a straight channel for which Eq. (55) gives $\Delta\overline{p}_0 = 12$ and $\Delta\overline{p}/\Delta\overline{p}_0 = 1$. Finally, as h_f approaches zero, $\Delta\overline{p}_0$ diverges to infinity as the gap at the outlet plane vanishes. For comparison, illustrative results produced from Eq. (55) are presented in the subsequent Section together with those obtained for an expanding/contracting tube.

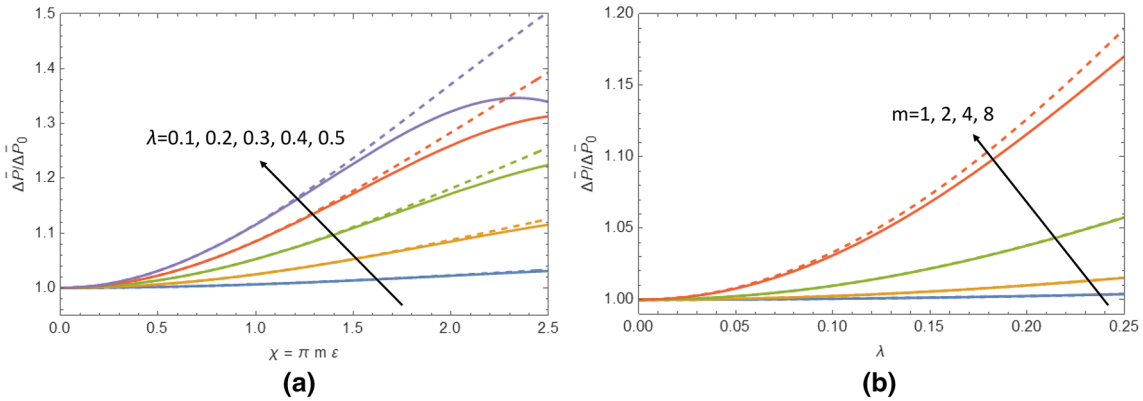

Fig. 4 The reduced average pressure drop for a tube with multiple constrictions (**a**) as function of $\chi = \pi\, m\, \varepsilon$ for various values of the amplitude of the constriction(s), λ; (**b**) as function of λ for m = 1, 2, 4, and 8. The aspect ratio is ε = 1/10. The corresponding results obtained using the acceleration formula, Eq. (52), are also shown dashed lines for comparison

4.2 Flow in a tube

For the flow in an axisymmetric tube of varying cross section, first we present the results for a wall with multiple constrictions. As for the channel flow, the shape function is given by $H(z) = 1 - \frac{\lambda}{2}(1 - \cos(2m\pi z))$ where the wavenumber m corresponds to the number of constrictions ($m = 1, 2, 3, ...$), and λ is their amplitude which is assumed to be the same for all constrictions and varies in the range $0 \le \lambda < 1$. Using $\chi \equiv \pi m\, \varepsilon$, the average pressure drop up to fourth order is found from Eqs. (51.1–3) as follows:

$$\Delta\overline{p} \approx \frac{(2-\lambda)\left(8-8\lambda+5\lambda^2\right)}{(1-\lambda)^{7/2}} + \frac{(2-\lambda)(4\lambda)^2}{3(1-\lambda)^{5/2}}\chi^2 + \frac{2\left(640\left(1-(1-\lambda)^{3/2}\right)+\lambda\left(41\lambda^2+238\lambda-960\right)\right)}{9(1-\lambda)^{3/2}}\chi^4. \tag{56}$$

It is clear that the pressure drop becomes unbounded as λ approaches unity, i.e., as the constriction(s) reach the axis of symmetry of the tube. In Fig. 4a, we show the predictions for the reduced average pressure drop, $\Delta\overline{p}/\Delta\overline{p}_0$, as function of χ for an increasing amplitude of the constriction(s). In the same Figure, the results obtained with the acceleration formula, $\Delta\overline{p}_S/\Delta\overline{p}_0$, are also shown for comparison. The increase of χ, which implies an increase in the number of constrictions and/or the increase in the tube aspect ratio, or the increase in the amplitude of the constriction(s), increase $\Delta\overline{p}/\Delta\overline{p}_0$. The increase is substantial and can reach up to 50% for the range of parameters shown in the Figure. Likewise, the results for a long undulating tube with aspect ratio $\varepsilon = 1/10$ are plotted as functions of the amplitude of the undulation in Fig. 4b. It is seen that the higher the wavenumber of the undulation, the higher the increase in the average pressure drop. Last, we emphasize that the great agreement of the original truncated perturbation solution with the acceleration formula gives confidence for the convergence and accuracy of the results.

For $\lambda < 0$, Eq. (56) can be used to study an undulating tube, and to compare with high accuracy numerical solutions from the literature [58, 59]. In these papers, the simulations were performed pseudospectrally for a fully periodic, along the main flow direction, undulating tube. Denoting the average radius of an equivalent straight circular tube by R, the wavelength of the undulation by L, and the amplitude of the undulation by αR, where α is dimensionless, the shape function for the wall was $r_w^*(x^*) = R(1 - \alpha\cos(2\pi x^*/L))$, $0 \le x^* \le L$ [58, 59]. Comparing r_w^* with the shape function used in the previous paragraph, i.e., $H^*(x^*) = h_0$ $(1 - (\lambda/2)(1 - \cos(2m\pi x^*/\ell)))$ (dimensional), one can confirm that the two formulations are equivalent provided that $\ell/m = L$, $\lambda = 2a/(a-1)$ and $m\,\varepsilon = (R/L)(1-\alpha)$. Since the calculations in Refs. [58, 59] were performed in a computational cell of length L, in our comparison we set $m = 1$. Thus, by defining a and R/L, we can calculate λ and ε. In Table 2, we compare the numerically obtained macroscopic dimensionless resistance of the flow, $f\mathrm{Re} \equiv 2\pi\ \Delta p^* R^4/(\eta\ q\ L)$, with the analytical results for $\Delta\overline{p}$ given by the classical lubrication theory, the high-order perturbation theory, Eq. (56), and the results derived by the acceleration formula, Eq. (52); note that by taking into account the relations between {λ, ε, m} and {a, R/L}, we find that $f\mathrm{Re} = m\ (1 - \lambda/2)^4\Delta\overline{p}$. It is seen that the high-order lubrication theory agrees very well with the numerical results. It is also very interesting that the quality of the agreement remains approximately the same for all the parameters shown in the Table. As far as the acceleration formula is concerned, it is important to note that in

Table 2 The dimensionless resistance to the flow, $f\mathrm{Re}$, as calculated in Refs. [58, 59] using spectral methods, compared to (a) the analytical results from the leading-order lubrication approximation (3rd column), (b) the results of Eq. (56) (4th column), and (c) the transformed results based on Eq. (52) (5th column)

Parameters	$f\mathrm{Re}$	$m\,(1-\lambda/2)^4\Delta\overline{p}_0$	$m\,(1-\lambda/2)^4\Delta\overline{p}$	$m\,(1-\lambda/2)^4\Delta\overline{p}_S$
$\alpha=0.100$, $R/L=0.5000$	17.74*	16.8214	17.7581	17.7748
$\alpha=0.200$, $R/L=0.1042$	19.7655	19.5649	19.7655	19.7655
$\alpha=0.300$, $R/L=0.1592$	26.4370	25.2622	26.4350	26.4365
$\alpha=0.286$, $R/L=0.2333$	26.3830	24.2155	26.3698	26.3809
$\alpha=0.500$, $R/L=0.5000$	95.6*	60.2155	77.3914	92.3348

*Indicates an approximate value extracted virtually from a figure in Ref. [59]

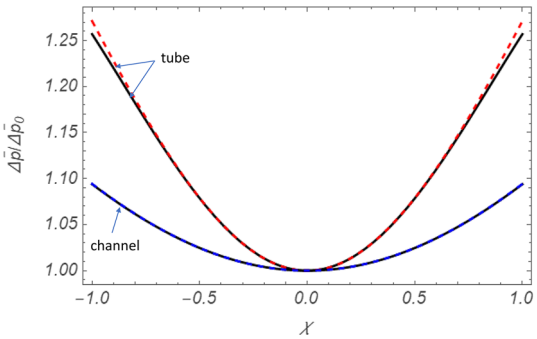

Fig. 5 The reduced average pressure drop for contracting ($\chi>0$) and expanding ($\chi<0$) tubes and for contracting ($\chi>0$) and expanding ($\chi<0$) channels. The corresponding results according to the acceleration formula, Eq. (52), are also shown with dashed lines (for the channel the results are indistinguishable). For both configurations, the contraction or expansion is linear

contrast to the cases presented for the undulating channel (see Table 1), Eq. (52) increases significantly the accuracy of Eq. (56), especially for $\alpha=0.5$ for which Eq. (56) does not agree well with the numerical results. All these observations clearly demonstrate the efficiency of the high-order lubrication theory, as well as the significance of the acceleration formula.

Last, we investigate a contracting/expanding tube whose wall is described by the linear shape function $H(z)=1+(h_f-1)z$ with $h_f>0$ being the radius of the outlet cross section. In this case, Eqs. (51.1–3) give

$$\frac{\Delta\overline{p}}{\Delta\overline{p}_0}\approx 1+\frac{1}{3}\chi^2-\frac{11}{144}\chi^4,\quad \Delta\overline{p}_0=\frac{16}{3}\left(\frac{1}{h_f}+\frac{1}{h_f^2}+\frac{1}{h_f^3}\right),\quad \chi\equiv(1-h_f)\varepsilon. \tag{57}$$

As previously found for a contracting/expanding symmetric channel, the sign of the modified aspect ratio χ does not matter since only even powers of χ appear in Eq. (57). Therefore, the reduced pressure drop is the same for both expanding and contracting tubes provided that $|\chi|$ is the same. Again, this feature is a consequence of the linearity of the Stokes equations, Eqs. (25–28), in conjunction with the fact that the contracting and expanding tubes are two mirror-image configurations of the same shaped body [2]. For $\chi=0$ (i.e., for $h_f=1=H(0)$) one gets a straight tube for which Eq. (57) gives $\Delta\overline{p}_0=16$ and $\Delta\overline{p}/\Delta\overline{p}_0=1$. As h_f approaches zero, $\Delta\overline{p}_0$ diverges to infinity as the radius of the outlet cross section vanishes. Illustrative results for $\Delta\overline{p}/\Delta\overline{p}_0$ (solid lines) and $\Delta\overline{p}_S/\Delta\overline{p}_0$ (dashed lines) are shown as functions of χ in Fig. 5, along with the corresponding results for the channel case (Eq. (55)). It is seen that for both the channel and the tube the higher-order terms in the lubrication approximation predict an increase in the average pressure drop; the increase is more significant for the flow in the tube. Also, the results shown using the acceleration formula are almost indistinguishable from the original truncated perturbation series (Eqs. (55) and (57)) indicating the high accuracy and convergence of the results.

Before closing this Section, we point out that the authors in Refs. [57–59] used extensively the domain perturbation method as an analytic technique to study the effect of the undulation of the boundary wall(s) on the dimensionless flow resistance, i.e., on $f\mathrm{Re}$. However, the agreement of the analytical results with the converged numerical results was reasonable only for very small amplitude of the undulation ($\alpha<0.1$, and in some cases even to as low as $\alpha=0.01$). On the contrary, the comparison that we performed in Tables 1 and 2 showed an extraordinary agreement of the high-order lubrication results, and the corresponding results

obtained with the acceleration formula, with the numerical results given in Refs. [57–59] for all values of the amplitude of the undulation, α.

5 Conclusions

Using a regular perturbation technique, we have systematically extended and generalized the classical lubrication theory for the creeping flow of a simple Newtonian fluid in confined and narrow configurations. High-order analytical results for the field variables (velocity and pressure) have been derived in channels with two variable walls and in tubes with varying circular cross section. The analysis is applicable provided that the shape functions that describe a-priori the geometry of the channel or tube are adequately smooth.

Focusing on the most interesting quantity for engineering applications, namely on the average pressure drop required to maintain the constant flowrate through the channel/tube, we have derived general expressions in terms of the aspect ratio and the shape functions (and their derivatives). For selected cases, such as contracting/expanding, undulating or rough channels and tubes, and configurations with multiple constrictions, analytical solutions for the average pressure drop have been derived and discussed. In all cases investigated, the effect of the higher-order terms is to increase the average pressure drop compared to that predicted by the classical leading-order lubrication theory. The magnitude of the increase, however, depends on the specific details and the parameters that characterize the geometry of the flow configuration.

In the cases of symmetric undulating channels and axisymmetric undulating tubes, comparison of the analytic results for the pressure drop with high-accurate numerical solutions from the literature showed excellent agreement between the solutions revealing the great accuracy and efficiency of the high-order lubrication theory. Furthermore, the comparison revealed the superiority of the theory against the domain perturbation method, especially for fully periodic configurations with large amplitude of the undulation. Finally, the implementation of the Shanks transformation and the Padé-type approximant(s) on the original truncated perturbation series further increased the accuracy of the analytical results, when these were compared to the numerical results, once again demonstrating the capability of these techniques to achieve better results than the original ones.

Acknowledgements We would like to thank Professor Antony N. Beris for his comments and suggestions on an earlier version of the paper and for bringing to our attention Refs. [57–59] which allowed us to demonstrate the accuracy and efficiency of the high-order lubrication theory.

Declarations

Conflict of interest The authors declare that they have no conflict of interest.

Appendix

For the channel flow, and using $G(x) \equiv H(x) + \Phi(x)$, the functions that appear in p_4 are:

$$\begin{aligned}
p_{4,0}(x) = \frac{1}{10G^4}(G-H)(&300H^3G'^3 + 60GH^2G'\left(G'^2 - 12G'H' - 3HG''\right)\\
&+3G^2H\left(-16G'^3 + 60G'^2H' + 60G'\left(H'^2 + HH''\right) + 5H\left(12H'G'' + HG^{(3)}\right)\right)\\
&+5G^5\left(G^{(3)} - 2H^{(3)}\right) + G^4\left(12H'G'' - 4G'\left(4G'' - 5H''\right) + H\left(G^{(3)} + 10H^{(3)}\right)\right)\\
&+G^3\left(24G'^3 + 12G'^2H' - 60G'\left(3H'^2 - H\left(G'' - 2H''\right)\right)\right.\\
&\left.+5\left(24H'^3 - 12HH'\left(2G'' - H''\right) - H^2\left(G^{(3)} + 4H^{(3)}\right)\right)\right)),\\
p_{4,1}(x) = -\frac{2}{5}&\left(84G'^3 - 132G'^2H' + 30H'^3 + 3GH'\left(5H'' + 6G''\right) + GG'\left(20H'' - 34G''\right) + G^2\left(4G^{(3)} - 5H^{(3)}\right)\right),\\
p_{4,2}(x) = \frac{3}{5}&\left(162G'^3 - 210G'^2H' + 10G'\left(3H'^2 + 4G\left(H'' - 2G''\right)\right) + G\left(10H'\left(4G'' + H''\right) + G\left(6G^{(3)} - 5H^{(3)}\right)\right)\right),\\
p_{4,3}(x) = -2&\left(48G'^3 - 36G'^2H' + 9GG'\left(H'' - 3G''\right) + G\left(9H'G'' + G\left(2G^{(3)} - H^{(3)}\right)\right)\right),\\
p_{4,4}(x) = &\,30G'^3 - 18GG'G'' + \frac{3}{2}G^2G^{(3)}.
\end{aligned}$$

Also, the functions that appear into $u_{x,4}$ are:

$$A_1(x) = -\frac{288}{5}G'^4 + \frac{768}{5}G'^3H' - \frac{G'^2}{15}\left(1800H'^2 + G\left(413H'' - 562G''\right)\right) + \frac{2}{15}G'\left(180H'^3 + 3GH'\left(65H'' - 148G''\right) + 2G^2\left(11H^{(3)} - 10G^{(3)}\right)\right) + \frac{G}{60}\left(60H'^2\left(19G'' + 4H''\right) + 24GH'\left(6G^{(3)} - 5H^{(3)}\right) + G\left(-80G''^2 + 148G''H'' - 30H''^2 + 8GG^{(4)} - 13GH^{(4)}\right)\right),$$

$$A_2(x) = \frac{504}{5}G'^4 - 192G'^3H' + \frac{3}{5}G'^2\left(140H'^2 + G\left(-142G'' + 79H''\right)\right) + \frac{2}{5}GG'\left(3H'\left(84G'' - 25H''\right) + 2G\left(11G^{(3)} - 8H^{(3)}\right)\right) + \frac{G}{20}\left(-420H'^2G'' - 8GH'\left(16G^{(3)} - 5H^{(3)}\right) + G\left(124G''^2 - 172G''H'' + 10H''^2 - 8GG^{(4)} + 9GH^{(4)}\right)\right),$$

$$A_3(x) = -72G'^4 + 72G'^3H' + \frac{18}{5}GG'^2\left(19G'' - 6H''\right) - \frac{6}{5}GG'\left(36H'G'' + G\left(7G^{(3)} - 3H^{(3)}\right)\right) + \frac{3}{20}G^2\left(-42G''^2 + 36G''H'' + 24H'G^{(3)} + 3GG^{(4)} - 2GH^{(4)}\right)$$

$$A_4(x) = 18G'^4 - 18GG'^2G'' + \frac{12}{5}G^2G'G^{(3)} + \frac{3}{20}G^2\left(12G''^2 - GG^{(4)}\right)$$

.

References

1. Langlois, W.E.: Slow Viscous Flow. Macmillan, New York (1964)
2. Leal, L.G.: Advanced Transport Phenomena: Fluid Mechanics and Convective Transport Processes. Cambridge University Press, Cambridge, UK (2007)
3. Ockendon, H., Ockendon, J.R.: Viscous Flow. Cambridge University Press, Cambridge, UK (1995)
4. Szeri, A.Z.: Fluid Film Lubrication: Theory and Design. Cambridge University Press, Cambridge, UK (2005)
5. Tichy, J. A.: Hydrodynamic lubrication, pp. 1–14. Boca Raton, FL: CRC Press (2012)
6. Goldman, A.J., Cox, R.G., Brenner, H.: Slow viscous motion of a sphere parallel to a plane wall—I. motion through a quiescent fluid. Chem. Eng. Sci. **22**, 637–651 (1967)
7. Stone, H.A.: On lubrication flows in geometries with zero local curvature. Chem. Eng. Sci. **60**, 4838–4845 (2005)
8. Amyot, O., Plouraboué, F.: Capillary pinching in a pinched microchannel. Phys. Fluids **19**, 033101 (2007)
9. Holmes, D.P., Tavakol, B., Froehlicher, G., Stone, H.A.: Control and manipulation of microfluidic flow via elastic deformations. Soft Matter **9**, 7049–7053 (2013)
10. Plouraboué, F., Geoffroy, S., Prat, M.: Conductances between confined rough walls. Phys. Fluids **16**, 615–624 (2004)
11. Stone, H.A., Stroock, A.D., Ajdari, A.: Engineering flows in small devices: microfluidics toward a lab-on-a-chip. Ann. Rev. Fluid Mech. **36**, 381–411 (2004)
12. Tavakol, B., Holmes, D.P.: Voltage-induced buckling of dielectric films using fluid electrodes. Appl. Phys. Lett. **108**, 112901 (2016)
13. Aboelkassem, Y., Staples, A.E.: Flow transport in a microchannel induced by moving wall contractions: a novel micropumping mechanism. Acta Mech. **223**, 463–480 (2012)
14. Aboelkassem, Y., Staples, A.E.: A bioinspired pumping model for flow in a microtube with rhythmic wall contractions. J. Fluid. Struct. **42**, 187–204 (2013)
15. Oron, A., Davis, S.H., Bankoff, S.G.: Long-scale evolution of thin liquid films. Rev. Mod. Phys. **69**, 931–980 (1997)
16. Snoeijer, J.H.: Free-surface flows with large slopes: beyond lubrication theory. Phys. Fluids **18**, 021701 (2006)
17. Bonn, D., Eggers, J., Indekeu, J., Meunier, J., Rolley, E.: Wetting and spreading. Rev. Mod. Phys. **81**, 739–805 (2009)
18. Limat, L., Stone, H.A.: Three-dimensional lubrication model of a contact line corner singularity. Europhys. Lett. **65**, 365–371 (2004)
19. Kalliadasis, S., Bielarz, C., Homsy, G.M.: Steady free-surface thin film flows over topography. Phys. Fluids **12**, 1889–1898 (2000)
20. Boyko, E., Stone, H.A.: Reciprocal theorem for calculating the flow-rate-pressure drop relation for complex fluids in narrow geometries. Phys. Rev. Fluids **6**, L081301 (2021)
21. Schomburg, W.K.: Introduction to Microsystem Design. Springer, Berlin (2011)
22. Sollier, E., Murray, C., Maoddi, P., Di Carlo, D.: Rapid prototyping polymers for microfluidic devices and high pressure injections. Lab Chip **11**, 3752–3765 (2011)
23. Ozsun, O., Yakhot, V., Ekinci, K.L.: Non-invasive measurement of the pressure distribution in a deformable micro-channel. J. Fluid Mech. **734**, R1 (2013)

24. Anoop, R., Sen, A.K.: Capillary flow enhancement in rectangular polymer microchannels with a deformable wall. Phys. Rev. E **92**, 013024 (2015)
25. Raj, A., Sen, A.K.: Flow-induced deformation of compliant microchannels and its effect on pressure–flow characteristics. Microfluid. Nanofluid. **20**, 31 (2016)
26. Gomez, M., Moulton, D.E., Vella, D.: Passive control of viscous flow via elastic snap-through. Phys. Rev. Lett. **119**, 144502 (2017)
27. Ando, K., Sanada, T., Inaba, K., Damazo, J.S., Shepherd, J.E., Colonius, T., Brenner, C.E.: Shock propagation through a bubbly liquid in a deformable tube. J. Fluid Mech. **671**, 339–363 (2011)
28. Pedley, T.J.: The Fluid Mechanics of Large Blood Vessels. Cambridge University Press, UK (1980)
29. Grotberg, J.B., Jensen, O.E.: Biofluid mechanics in flexible tubes. Ann. Rev. Fluid Mech. **36**, 121–147 (2004)
30. Popel, A.S., Johnson, P.C.: Microcirculation and hemorheology. Ann. Rev. Fluid Mech. **37**, 43 (2005)
31. Sebastian, B., Dittrich, P.S.: Microfluidics to mimic blood flow in health and disease. Ann. Rev. Fluid Mech. **50**, 483 (2018)
32. Allmendinger, A., Fischer, S., Huwyler, J., Mahler, H.C., Schwarb, E., Zarraga, I.E., Mueller, R.: Rheological characterization and injection forces of concentrated protein formulations: An alternative predictive model for non-Newtonian solutions. Eur. J. Pharm. Biopharm. **87**, 318 (2014)
33. Fischer, I., Schmidt, A., Bryant, A., Besheer, A.: Calculation of injection forces for highly concentrated protein solutions. Int. J. Pharm. **493**, 70 (2015)
34. Tavakol, B., Froehlicher, G., Holmes, D.P., Stone, H.A.: Extended lubrication theory: Improved estimates of flow in channels with variable geometry. Proc. R. Soc. A **473**, 20170234 (2017)
35. Hinojosa, R.B.C., Phan, K., Rouby, C.: Extension of the lubrication theory for arbitrary wall shape: An asymptotic analysis. C.R. Mec. **347**, 389–396 (2019)
36. Disimile, P., Wang, C.Y.: The forces due to the relative motion of two corrugated plates. Phys. Fluids **26**, 611–613 (1983)
37. Wang, C.Y.: Drag due to a striated boundary in slow Couette flow. Phys. Fluids **21**, 697–698 (1978)
38. Wang, C.Y.: Stokes flow through a channel with three-dimensional bumpy walls. Phys. Fluids **16**, 2136–2139 (2004)
39. Hasegawa, E., Izuchi, H.: On steady flow through a channel consisting of an uneven wall and a plane wall: part 1. case of no relative motion in two walls. Bull. JSME **26**, 514–520 (1983)
40. Hemmat, M., Borhan, A.: Creeping flow through sinusoidally constricted capillaries. Phys. Fluids **7**, 2111–2121 (1995)
41. Malevich, A.E., Mityushev, V.V., Adler, P.M.: Stokes flow through a channel with wavy walls. Acta Mech. **182**, 151–182 (2006)
42. Manton, M.J.: Low Reynolds number flow in slowly varying axisymmetric tubes. J. Fluid Mech. **49**, 451–459 (1971)
43. Stoker, J.J.: Water Waves. Interscience, New York (1957)
44. Joseph, D.: Parameter and domain dependence of eigenvalues of elliptic partial differential equations. Arch. Rat. Mech. Anal. **24**, 325–351 (1967)
45. Joseph, D.: Domain perturbations: The higher order theory of infinitesimal water waves. Arch. Rat. Mech. Anal. **51**, 295–303 (1973)
46. Wolfram Research Inc., Mathematica Edition: Version 12, Champaign, Illinois, (2019)
47. Bender, C.M., Orszag, S.A.: Advanced Mathematical Methods for Scientists and Engineers I-Asymptotic Methods and Perturbation Theory, 1st edn. Springer-Verlag, New York (1999)
48. Housiadas, K.D.: Improved convergence based on linear and non-linear transformations at low and high Weissenberg asymptotic analysis. J. Non-Newtonian Fluid Mech. **247**, 1–14 (2017)
49. Shanks, D.: Non-linear transformations of divergent and slowly convergent sequences. J. Math. and Phys. **34**, 1–42 (1955)
50. Van Dyke, M.: Perturbation methods in fluid mechanics. The Parabolic Press, Stanford (1964)
51. H. Padé. Sur la representation approachee d'une function pour des functions rationeless. Thesis Ecole Normal Sup, (1892)
52. Faroughi, S.A., Fernandes, C., Nóbrega, J.M., McKinley, G.H.: A closure model for the drag coefficient of a sphere translating in a viscoelastic fluid. J. Non-Newtonian Fluid Mech. **277**, 104218 (2020)
53. Gkormpatsis, S.D., Gryparis, E.A., Housiadas, K.D., Beris, A.N.: Steady slip translation in a viscoelastic fluid with slip on the surface of the sphere. J. Non-Newtonian Fluid Mech. **275**, 104217 (2020)
54. Housiadas, K.D.: Steady sedimentation of a spherical particle under constant rotation. Phys. Rev. Fluids **4**, 103301 (2019)
55. Housiadas, K.D., Tanner, R.I.: Viscoelastic shear flow past an infinitely long and freely rotating cylinder. Phys. Fluids **30**, 073101 (2018)
56. Zhang, A., Murch, W.L., Einarsson, J., Shaqfeh, E.S.G.: Lift and drag force on a spherical particle in a viscoelastic shear flow. J. Non-Newtonian Fluid Mech. **220**, 10479 (2020)
57. Beris, A.N., Avgousti, M., Souvaliotis, A.: Spectral calculations of viscoelastic flows: evaluation of the Giesekus constitutive equation in model flow problems. J. Non-Newtonian Fluid Mech. **44**, 197–228 (1992)
58. Pilitsis, S., Beris, A.N.: Calculations of steady-state viscoelastic flow in an undulating tube. J. Non-Newtonian Fluid Mech. **31**, 231–287 (1989)
59. Pilitsis, S., Beris, A.N.: Viscoelastic flow in an undulating tube. part II. effects of high elasticity, large amplitude of undulation and inertia. J. Non-Newtonian Fluid Mech. **39**, 375–405 (1991)